

Cold wall CVD generation of single-walled carbon nanotubes and in situ Raman scattering measurements of the growth stage

Shohei Chiashi, Yoichi Murakami, Yuhei Miyauchi, Shigeo Maruyama*

*Department of Mechanical Engineering, The University of Tokyo
7-3-1 Hongo, Bunkyo-ku, Tokyo 113-8656, Japan*

Received 20 October 2003; in final form 18 December 2003

*Corresponding Author. Fax: +81-3-5800-6983.

E-mail address: maruyama@photon.t.u-tokyo.ac.jp (S. Maruyama).

Abstract

Catalytic CVD generation of high-purity single-walled carbon nanotubes (SWNTs) without use of an electric furnace or a hot-filament is demonstrated. High-purity SWNTs were generated from alcohol used as a carbon source with Fe/Co particles supported on zeolite by Joule- heating of a silicon base plate. This technique was applied for an in situ measurement of Raman scattering during the growth stage in a vacuum chamber equipped with an SPM/Raman detector. The surface temperature was measured by a systematic shift in the silicon signal and kept at 850 °C. The G-band intensity of the SWNT Raman spectrum increased nearly linearly with time in the growth stage after an initial rapid increase.

1. Introduction

The discovery of single-walled carbon nanotubes (SWNTs) [1] has invoked numerous research interests because of their unique physical properties [2] and hence remarkable potential as a new material for various applications. The generation technique of SWNTs has since been developed by demands for specimens with sufficient amount and quality. Followed by the landmark establishment of the synthesis method in macroscopic amounts by laser-furnace [3] and arc-discharge [4] methods, several techniques employing the CVD approach [5-13] have been proposed for improved efficiency or productivity in the bulk synthesis of SWNTs. At present, CVD approaches, including the high-pressure CO (HiPco) technique [6, 7], have become dominant for the mass production of SWNTs.

As a new approach for higher-purity and lower-temperature generation, we have proposed the use of alcohol, particularly ethanol and methanol, for the carbon feedstock [14, 15]. The proposed alcohol catalytic CVD (ACCVD) method can produce high-quality SWNTs when combined with appropriate catalysts and experimental procedures. Furthermore, it was recently demonstrated that high-quality SWNTs could be synthesized on a mesoporous-silica coated substrate [16] or directly on a solid substrate such as silicon or quartz [17, 18]. Detailed comparisons of HiPco and ACCVD products are found in our recent papers [19, 20], and the generation mechanism is discussed based on molecular

dynamics simulations [21]. Another advantage of ACCVD is simplicity and safety of its implementation. The use of alcohol is now feasible for the direct growth of SWNTs on metal electrodes or on Si substrates for manufacturing FET devices from directly grown nanotubes [22]. Furthermore, Okazaki et al. [23] have demonstrated hot-filament CVD using ethanol for a simpler generation technique.

In this report, an even simpler version of ACCVD without resort to an electric furnace or a hot filament is proposed. All one needs is a vacuum chamber with a rotary pump and a hot plate to heat up the catalyst. Growth of SWNTs has been demonstrated by using Fe/Co metal particles supported on zeolite. Since this CVD apparatus is so simple, we have further achieved in situ observation of Raman scattering during the SWNT growth stage.

2. Preparations and Experiments

Details of the preparation of metal-supporting zeolite powder are described elsewhere [14, 15]. Catalytic powder was prepared by impregnating USY-zeolite powder (HSZ-390HUA over 99 % SiO₂) with iron acetate (CH₃CO₂)₂Fe and cobalt acetate (CH₃CO₂)₂Co·4H₂O [24, 25]. The weight concentrations of Fe and Co were chosen to be 2.5 wt % each over the catalytic powder.

A simple CVD apparatus was used with an electric furnace, a quartz tube, and a vacuum rotary pump [14, 15]. However, we found that keeping the ethanol vapor at high CVD temperature was inessential for SWNTs growth. All that we needed were a vacuum chamber and a small heater inside the chamber, as shown in Fig. 1(a). We supplied ethanol vapor from a reservoir at room temperature through an ethanol gas port, and we installed an optical system that can focus laser light to a 2 μm spot and collect scattered light through a top observation window. For measurement of Raman scattering in situ, we selected a vacuum chamber unit for a scanning probe microscope (SPM), SII SPA 300HV. A typical 2 mW Raman excitation laser was used. This optical system was connected with a Raman system via optical fibers. For micro-Raman scattering measurements, CHROMEX 501IS and ANDOR DV401-FI spectrometers and a CCD system with a SEKI TECHNOTRON STR250 optical system were used.

A Joule heater was used for the catalysts, as shown in Fig. 1(b), with an ac voltage supplied to a silicon substrate (Nilaco, 100, p-type, 20 × 5 × 0.5 mm) through a voltage regulator. Zeolite powder supporting Fe/Co nano-particles was placed on the silicon base. The zeolite particles were dispersed in ethanol, and a drop of about 0.5 μL was dried on the silicon substrate. Typical resistance of the substrate including the contact resistance, 100 Ω before heating, was decreased to ≈ 5 Ω after heating due to the reduction in the contact resistance.

After evacuating the chamber to 0.1 Torr, an ac voltage (typically 6 V) was applied to the silicon plate. The surface temperature of the silicon plate was monitored by the calibrated change of the silicon Raman shift, ≈ 520 cm⁻¹, to be reported in the next section. After application of this voltage, the surface temperature of the silicon plate increased to the growth temperature, typically 850 °C, in ≈ 1 min. Then, ethanol vapor at 1 Torr was supplied through a needle valve. To keep the surface temperature constant, the ac voltage was slightly adjusted by monitoring the silicon Raman shift. After a certain CVD period, the ethanol supply was stopped, the chamber was evacuated for 4 min, and the heating power was turned off. Since no Ar buffer gas was present in the supply line, this procedure was essential for the generation of high-purity SWNTs. Exposure of ethanol vapor to lower temperature catalysts during the

heating-up or cooling-down resulted in considerable generation of amorphous carbon. With a supply line of buffer gas such as Ar or Ar/H₂, standard ACCVD procedures [14, 15] were usable. The produced samples were characterized by FE-SEM (Hitachi S-900) and TEM (JEM2000FX at 120 kV) in addition to Raman scattering.

3. Results and discussion

3.1. Cold wall CCVD generation of SWNTs

The Raman scattering of SWNTs generated by the cold wall CCVD is shown in Fig. 2(a). A sharp, branched G-band signal at $\approx 1590\text{ cm}^{-1}$, a very small D-band signal at $\approx 1350\text{ cm}^{-1}$, and a radial breathing mode (RBM) around $150\text{-}300\text{ cm}^{-1}$ are typical features of SWNTs [26, 27]. High purity of SWNTs generated by this process is evident in contrast with a normal ACCVD sample [15] (Fig. 2(b)) and a HiPco sample, supplied by Rice University with batch #HPR113.4 (Fig. 2(c)). The diameter d of SWNTs was estimated from the RBM Raman shift ν using the relationship $d/\text{nm} = 248 / (\nu/\text{cm}^{-1})$ on the top axis of Fig. 2 [28, 29]. By comparison of the RBM signal in Fig. 2 with the temperature-dependent diameter distribution of the ACCVD sample [14], the effective reaction temperature was estimated to be slightly higher than $850\text{ }^\circ\text{C}$. We observed a larger D-band signal in the Raman scattering of the sample (not shown) generated by a wrong heating-up procedure (i.e. a supply of ethanol vapor during the heating-up of silicon plate). Because of the low temperature reaction during this heating-up, a considerable amount of amorphous carbon was generated. The yield of SWNTs was not measured for this sample, but the catalyst powder looked black after 20 min of CVD reaction.

SWNTs were further characterized by SEM and TEM observations. For a SEM measurement, the silicon substrate was directly mounted on a SEM sample holder. In the SEM image of this sample measured at 5 kV, shown in Fig. 3(a), bundles of SWNTs were observed as thin web-like structures between zeolite particles of about 300 nm. Morphology of SWNTs was similar to our previous observations of standard ACCVD samples [14, 19], though the amount of SWNTs was much less due to the lower ethanol pressure and no Ar/H₂ gas. The ‘as grown’ sample was mildly sonicated in methanol for 1 min and a drop was dried on a grid for TEM observation. The absence of metal particles or multi-wall carbon nanotubes in Fig. 3(b) evidences high purity of these SWNTs. In comparison with the high-quality standard ACCVD sample [14, 19], a small amount of amorphous carbon attached to the side walls was noticed, and the bundle size was found to be thinner.

Since simple heating of the catalyst can generate high-purity SWNTs, a much simpler ACCVD procedure can be proposed. Without a surrounding electric furnace, no preheating of the ethanol is essential. It is also evident that no gas-phase decomposition of ethanol is necessary for ACCVD generation of SWNTs. Hot-filament CVD [23] using ethanol seems to contradict this finding. However, a hot filament was always positioned so close to the catalysts in those experiments that catalysts may have been heated effectively.

3.2. Temperature dependence of Raman shifts of silicon peak and G-band

Figure 4(a) shows the temperature dependence of Raman scattering from ‘as grown’ SWNTs supported on zeolite and mounted on the silicon substrate. After the cold wall CCVD generation, the sample was heated again in vacuum and Raman scattering was measured at different temperatures for

calibration of subsequent in-situ measurements. Significant decreases were observed in the G-band and the silicon peak signals with increasing temperature. At the same time, softening (i.e., down frequency shift) of these vibrations was clearly observed, as shown in Fig. 4(b) in comparison with several previous reports [30-32]. In micro-Raman measurements, the temperature of the laser spot was determined by a balance between the heat input of the laser and the cooling by heat transfer from the laser spot to the environment. For a silicon substrate, however, this extra laser heating is negligible because of the efficient heat conduction to bulk substrate and cancellation of anharmonic softening shift by the compressive stress due to the surrounding substrate [33]. As shown in Fig. 4(b) the Raman shift for pure silicon substrate measured with a thermocouple agreed well with the data and the semi-empirical curve reported by Balkanski et al. [32]. Hence, the softening of the silicon peak position is especially useful for the in situ measurement of surface temperature merely by use of the Raman scattering signal. On the other hand, an extra laser heating effect was observed for a nanotube sample when a higher power density was used [30]. When a laser with a power density as small as 6×10^4 W/cm² (2 mW at 2 μ m beam diameter) was used in our study, our results in Fig. 3(b) was similar to those reported in Ref. [30], but an appreciably different value has also been reported [31]. As the reason for this discrepancy is yet unknown, we have used the G-band shift as a rough estimate of temperature in the present Letter.

3.3. In situ Raman scattering measurements during SWNT growth

In the cold wall CCVD process, the excitation laser was continuously irradiated to the sample, and Raman scattering was measured at every second. A gradual increase in the G-band signal at ≈ 1566 cm⁻¹ is clearly observed in the instantaneous Raman signal, shown in Fig. 5(a), as an average of each minute. The G-band peak, which appears at a lower frequency, implies that the reaction temperature was around 930 °C by a linear extrapolation of data in Fig. 4(b). The instantaneous G-band intensity and the Raman shift are compared with the silicon peak intensity and the silicon peak shift in Fig. 5(b). Soon after heating of the silicon plate, a red shift and a rapid decrease in intensity of the silicon peak was observed. Since there was no G-band peak, the detected Raman shift of the G-band was just a random scatter in the bottom panel. After the exposure to ethanol vapor, practically no change in the silicon peak was observed, showing that the surface temperature was kept nearly constant. On the other hand, a rapid increase in the G-band, followed by an essentially linear increase in intensity, was observed. Since the temperature was kept constant, the G-band shift also remained constant. After stopping the flow of ethanol vapor, there was still some increase in the G-band intensity. After the heating voltage was turned off, a shift and a rapid increase in the intensity were observed in the silicon and G-band signals due to cooling of the sample. During this cooling stage, a gradual increase in the G-band signal was observed after a rapid increase, being consistent with a temperature-dependent change in the Raman shift.

The observed linear increase in the G-band signal without an incubation time (delay of growth) during the CCVD process is consistent with our previous TGA observations [15], where a linear increase in the SWNT yield with the CVD time was measured. The linear increase in the amount of SWNTs can be explained by one of the two possible mechanisms: either a linear increase in the length of each nanotube or that in the number of nanotubes, or both. A further study using an AFM in this chamber may provide a clue.

Acknowledgements

The authors thank Mr. H. Tsunakawa and Mr. T. Ito (UT) for assistance in TEM measurements, Prof. T. Okubo and Mr. T. Sugawara (UT) for helping FE-SEM measurements, Prof. R. E. Smalley (Rice University) for supplying HiPco sample, and Mr. Erik Einarsson (UT) for discussions. Part of this work was financially supported by KAKENHI #13555050 and #15-11652 from JSPS, and #13GS0019 from MEXT.

References

- [1] S. Iijima, T. Ichihashi, *Nature* 363 (1993) 603.
- [2] R. Saito, G. Dresselhaus, M.S. Dresselhaus, *Physical Properties of Carbon Nanotubes*, Imperial College Press, London, 1998.
- [3] A. Thess, R. Lee, P. Nikolaev, H. Dai, P. Petit, J. Robert, C. Xu, Y.H. Lee, S.G. Kim, A.G. Rinzler, D.T. Colbert, G.E. Scuseria, D. Tománek, J.E. Fischer, R.E. Smalley, *Science* 273 (1996) 483.
- [4] C. Journet, W.K. Maser, P. Bernier, A. Loiseau, M.L. de la Chapelle, S. Lefrant, P. Deniard, R. Lee, J.E. Fischer, *Nature* 388 (1997) 756.
- [5] H. Dai, A.G. Rinzler, P. Nikolaev, A. Thess, D.T. Colbert, R.E. Smalley, *Chem. Phys. Lett.* 260 (1996) 471.
- [6] P. Nikolaev, M.J. Bronikowski, R.K. Bradley, F. Rohmund, D.T. Colbert, K.A. Smith, R.E. Smalley, *Chem. Phys. Lett.* 313 (1999) 91.
- [7] M.J. Bronikowski, P.A. Willis, D.T. Colbert, K.A. Smith, R.E. Smalley, *J. Vac. Sci. Technol. A* 19 (2001) 1800.
- [8] J.-F. Colomer, J.-M. Benoit, C. Stephan, S. Lefrant, G. Van Tendeloo, J.B. Nagy, *Chem. Phys. Lett.* 345 (2001) 11.
- [9] B. Zheng, Y. Li, J. Liu, *Appl. Phys. A* 74 (2002) 345.
- [10] W.E. Alvarez, F. Pompeo, J.E. Herrera, L. Balzano, D.E. Resasco, *Chem. Mater.* 14 (2002) 1853.
- [11] A.R. Harutyunyan, B.K. Pradhan, U.J. Kim, G. Chen, P.C. Eklund, *Nano Lett.* 2 (2002) 525.
- [12] Y. Zhang, A. Chang, J. Cao, Q. Wang, W. Kim, Y. Li, N. Morris, E. Yenilmez, J. Kong, H. Dai, *Appl. Phys. Lett.* 79 (2001) 3155.
- [13] S. Huang, X. Cai, J. Liu, *J. Am. Chem. Soc.* 125 (2003) 5636.
- [14] S. Maruyama, R. Kojima, Y. Miyauchi, S. Chiashi, M. Kohno, *Chem. Phys. Lett.* 360 (2002) 229.
- [15] Y. Murakami, Y. Miyauchi, S. Chiashi, S. Maruyama, *Chem. Phys. Lett.* 374 (2003) 53.
- [16] Y. Murakami, S. Yamakita, T. Okubo, S. Maruyama, *Chem. Phys. Lett.* 375 (2003) 393.
- [17] Y. Murakami, Y. Miyauchi, S. Chiashi, S. Maruyama, *Chem. Phys. Lett.* 377 (2003) 49.
- [18] Y. Murakami, S. Chiashi, Y. Miyauchi, M. Hu, M. Ogura, T. Okubo, S. Maruyama, *Chem. Phys. Lett.* in press.
- [19] S. Maruyama, Y. Miyauchi, Y. Murakami and S. Chiashi, *New J. Phys.* 5 (2003) 149.1.
- [20] Y. Miyauchi, S. Chiashi, Y. Murakami, Y. Hayashida, S. Maruyama, *Chem. Phys. Lett.*, submitted.
- [21] Y. Shibuta, S. Maruyama, *Chem. Phys. Lett.* 382 (2003) 381.

- [22] Y. Ohno, S. Iwatsuki, T. Hiraoka, T. Okazaki, S. Kishimoto, K. Maezawa, H. Shinohara, T. Mizutani, *Jpn. J. Appl. Phys.* 42 (2003) 4116.
- [23] T. Okazaki, H. Shinohara, *Chem. Phys. Lett.* 376 (2003) 606.
- [24] K. Mukhopadhyay, A. Koshio, N. Tanaka, H. Shinohara, *Jpn. J. Appl. Phys.* 37 (1998) L1257.
- [25] K. Mukhopadhyay, A. Koshio, T. Sugai, N. Tanaka, H. Shinohara, Z. Konya, J. B. Nagy, *Chem. Phys. Lett.* 303 (1999) 117.
- [26] A.M. Rao, E. Richter, S. Bandow, B. Chase, P.C. Eklund, K.A. Williams, S. Fang, K.R. Subbaswamy, M. Menon, A. Thess, R.E. Smalley, G. Dresselhaus, M.S. Dresselhaus, *Science* 275 (1997) 187.
- [27] M.S. Dresselhaus, P.C. Eklund, *Advances in Physics*, 49 (2000) 705.
- [28] R. Saito, G. Dresselhaus, M.S. Dresselhaus, *Phys. Rev. B* 61 (2000) 2981.
- [29] A. Jorio, R. Saito, J.H. Hafner, C.M. Lieber, M. Hunter, T. McClure, G. Dresselhaus, M.S. Dresselhaus, *Phys. Rev. Lett.* 86 (2001) 1118.
- [30] H.D. Li, K.T. Yue, Z.L. Lian, Y. Zhan, L.X. Zhou, S.L. Zhang, Z.J. Shi, Z.N. Gu, B.B. Liu, R.S. Yang, H.B. Yang, G.T. Zou, Y. Zhang, S. Iijima, *Appl. Phys. Lett.* 76 (2000) 2053.
- [31] N.R. Raravikar, P. Keblinski, A.M. Rao, M.S. Dresselhaus, L.S. Schadler, P.M. Ajayan, *Phys. Rev. B* 66 (2002) 235424.
- [32] M. Balkanski, R.F. Wallis, E. Haro, *Phys. Rev. B* 28 (1983) 1928.
- [33] S. Kouteva-Arguirova, Tz. Arguirov, D. Wolfframm, J. Reif, *J. Appl. Phys.* 94 (2003) 4946.

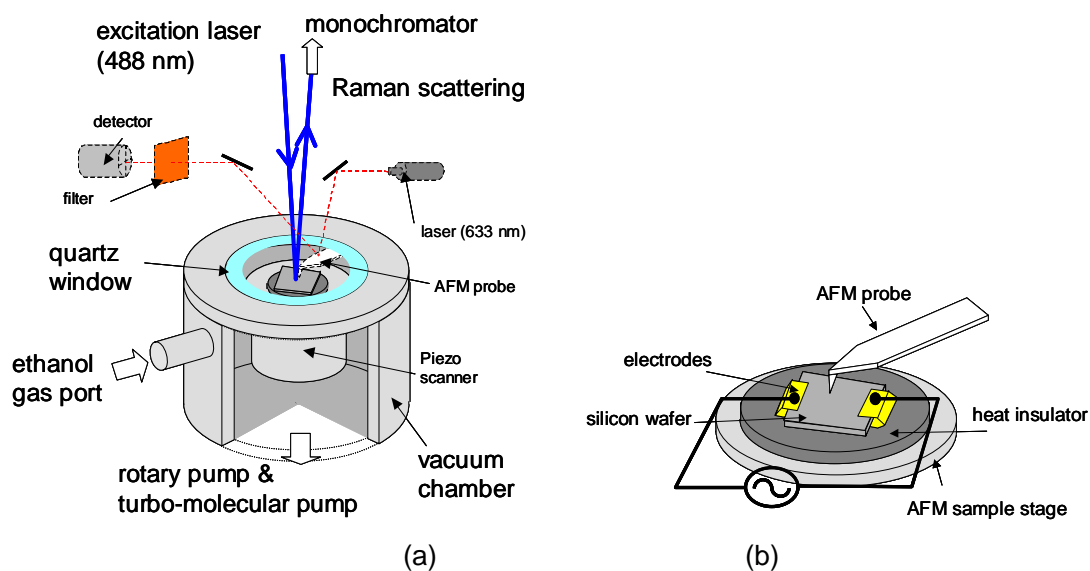


Fig. 1. Schematics of the experimental apparatus. (a) Set-up for in situ measurement of Raman scattering during SWNTs growth. Note that the 633 nm laser/detector and AFM probe have not been used in this Letter. (b) A magnified image of the silicon sample heated by Joule heating.

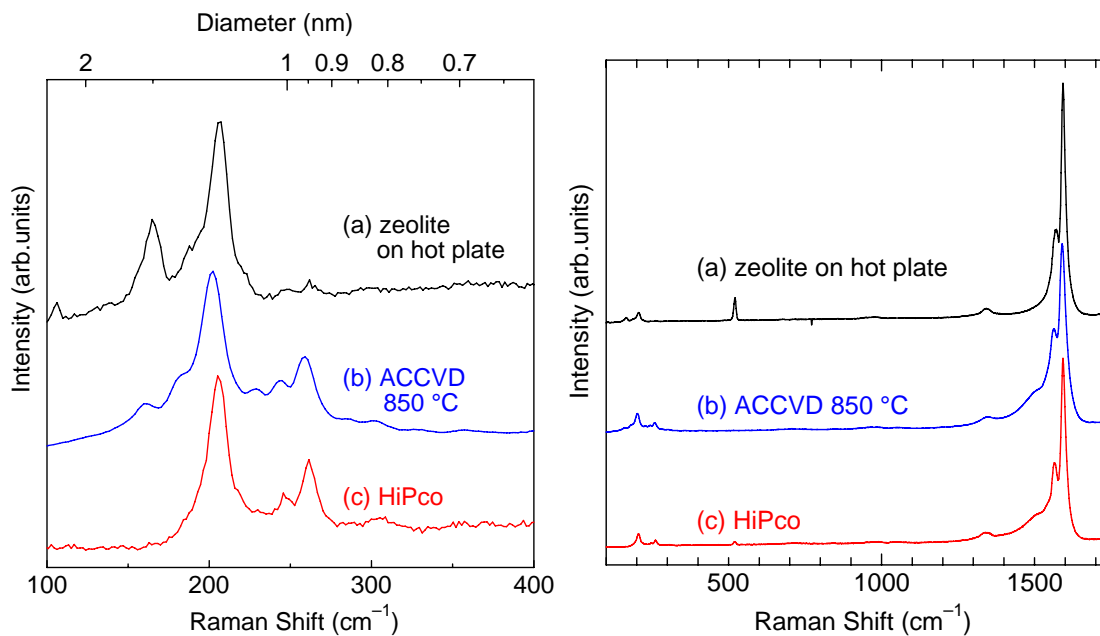
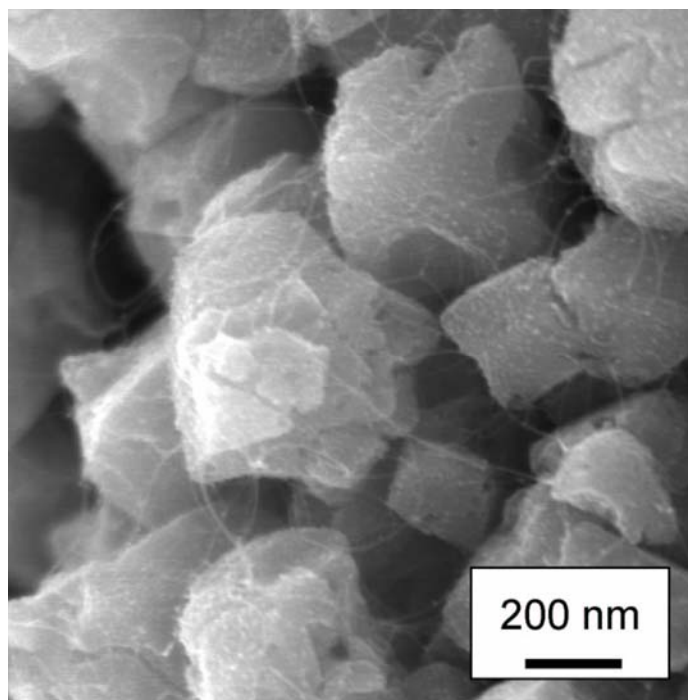
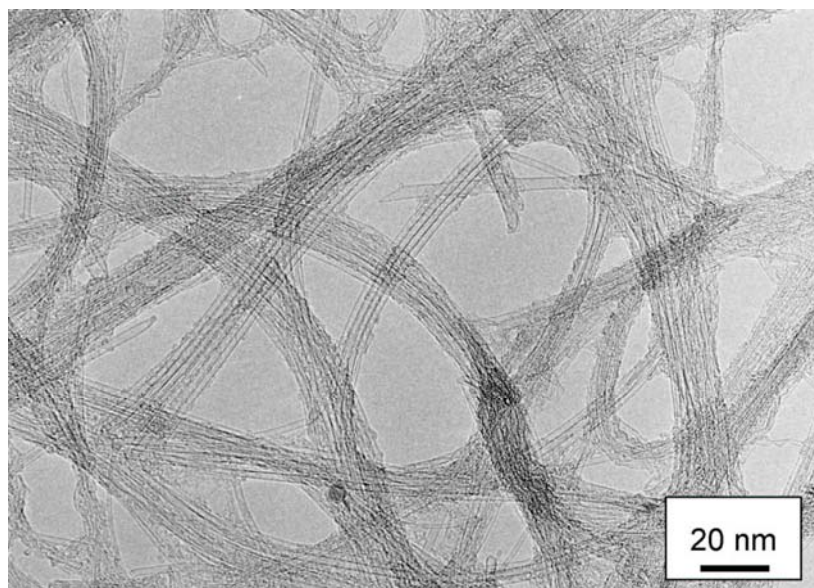


Fig. 2. Raman scattering spectra measured by 488 nm laser excitation. The right panel shows full range, and the left panel is a magnification of the radial breathing mode (RBM). (a) Fe/Co on zeolite. (b) Conventional ACCVD at 850 °C. (c) HiPco sample.



(a)



(b)

Fig. 3. (a) SEM and (b) TEM images of SWNTs generated by cold wall CCVD.

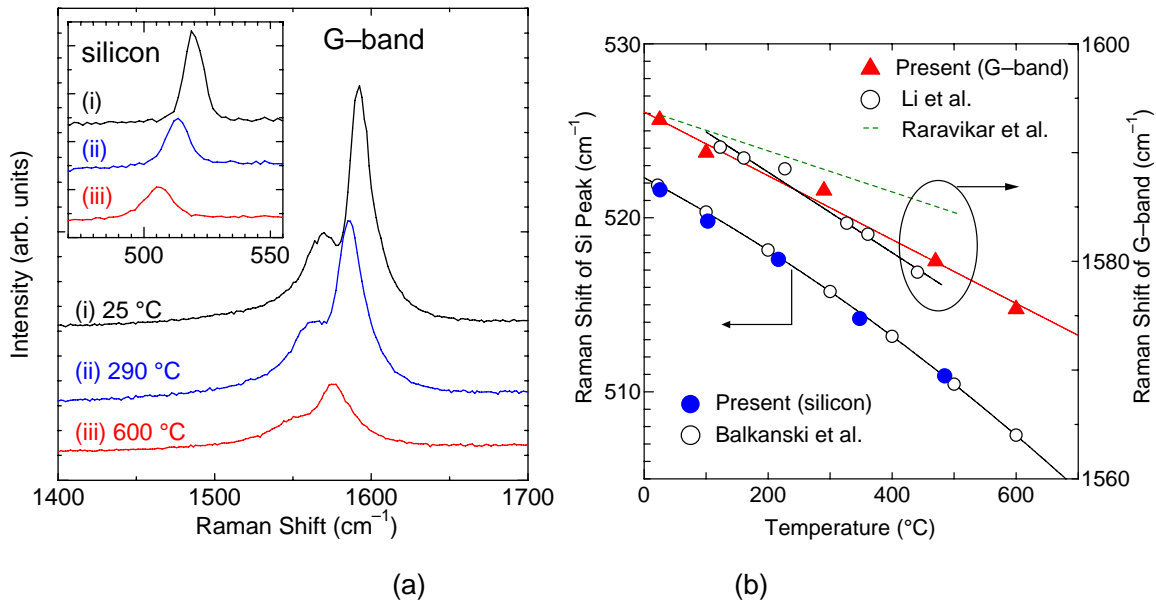


Fig. 4. (a) Temperature dependence of Raman scattering of SWNTs grown by cold wall ACCVD. (b) Temperature dependences of the Raman shifts for silicon and G-band peaks. Silicon peaks were measured with a plain silicon surface with a thermocouple. The surface temperature of silicon substrate loaded with SWNTs was determined by using this correlation.

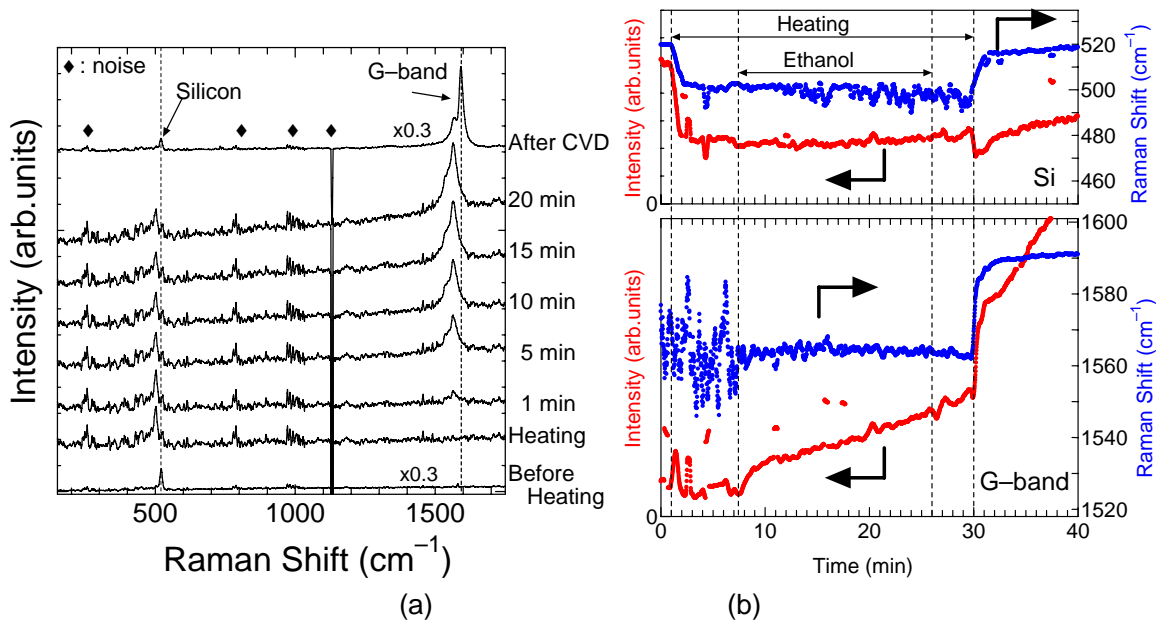


Fig. 5. In-situ measurement of Raman scattering during ACCVD process. (a) Examples of instantaneous Raman scattering signals during the growth stage of SWNTs. Spectra are based on 1 min averages. (b) Instantaneous changes in the G-band intensity and Raman shift vs. silicon signals used for estimation of surface temperature.